

Electronic Supplementary Information

Characterizations

X-ray diffraction (XRD) data were acquired on a D/MAX 2550 diffractometer with Cu K α radiation from 5° to 80° ($\lambda = 1.5418 \text{ \AA}$). Scanning electron microscopy (SEM) measurements were carried out on a XL30 ESEM FEG scanning electron microscope at an accelerating voltage of 20 kV and energy dispersive X-ray detector (EDX) was characterized by using a JEOLJSM-6700F. Transmission electron microscopy (TEM) high-resolution TEM (HRTEM) data was performed on a JEOL JEM2100 electron microscopy with an accelerating voltage of 200 kV. X-ray photoelectron spectroscopy (XPS) data were acquired on an ESCALAB 250 X-ray photoelectron spectrometer (Thermo Fisher Scientific, USA) with C 1s peak (binding energy of 284.8 eV) as reference. The Brunauer-Emmett-Teller (BET) surface area of the samples was performed on an ASAP2460 analyzer. The mass loading was obtained by weighing on an electronic analytical balance of AL 204. Raman spectra were recorded on a Raman spectrometer (Horiba LabRAM HR Evolution) with 532 nm laser excitation.

Electrochemical measurements

The electrochemical performance measurements were performed on a CHI660D electrochemistry analyzer (CH Instruments, Inc., Shanghai) in a three-electrode system using the CoMoO₄@CoFe/NF, graphite rod and Hg/HgO electrode as working electrode, counter electrode and reference electrode, respectively. All the electrochemical performance measurements were carried out in 1.0 M KOH aqueous

electrolyte. All the potential data reported in this work were converted to reversible hydrogen electrode (RHE) according to the E-1. Polarization curves were obtained through linear sweep voltammetry (LSV) from 1 to 2 V vs. RHE at a scan rate of 2 mV s⁻¹. The Tafel plots are employed to evaluate the OER catalytic kinetics and obtained from the corresponding LSV curves (E-2). The EIS tests were recorded at open-circuit potential with a frequency range from 0.1 Hz to 100 kHz. Long-term stability was tested via chronoamperometry. The electrochemical surface area (ECSA) was calculated according to the E-3. A constant current of 50 mA was applied to a two-electrode electrolytic cell with an electrode area of 0.25 cm² for about 150 min to collect oxygen and the gas collection device is shown in Fig. S8a. The faraday efficiency (FE) is calculated by comparing experimental and theoretical gas production under ideal gas conditions. Double-layer capacitance (C_{dl}) measurements were conducted by CV scanning from 0.795 to 0.845 V with different scan rates (20, 40, 60, 80 and 100 mV s⁻¹). The slope of Δj vs. scan rate curve is twice of C_{dl} , where Δj is $j_a - j_c$ corresponding to the current density difference at the middle potential of CV potential (0.82 V).

$$E(\text{RHE}) = E(\text{Hg/HgO}) + 0.098 + 0.059 \times \text{pH} - i \times R_s \quad (\text{E-1})$$

Where i is the current density (mA cm⁻²) and R_s is the series resistance obtained from the electrochemical impedance spectroscopy (EIS) measurements. The value of R_s was 2.5 in 1.0 M KOH in this work.

$$\eta = b \log j + a \quad (\text{E-2})$$

Where j is the current density and b is the Tafel slope.

$$i_p = 0.4463 \times 10^{-3} \times n^{3/2} \times F^{3/2} \times A \times C_{R^*} \times D_R^{1/2} \times \nu^{1/2} \times (RT)^{-1/2} \quad (\text{E-3})$$

Where n is the number of electrons transferred of potassium ferricyanide ($n = 1$), F is Faraday constant (96485 C mol^{-1}), R is the gas constant ($8.314 \text{ J mol}^{-1} \text{ K}^{-1}$), T is the temperature (298 K), C_{R^*} (mol L^{-1}) is the potassium ferricyanide concentration (5 mM) and ν is the CV scan rate (0.02 V s^{-1}). The diffusion coefficient (D_R) of potassium ferricyanide was based on the reference data ($7.6 \times 10^{-6} \text{ cm}^2 \text{ s}^{-1}$).

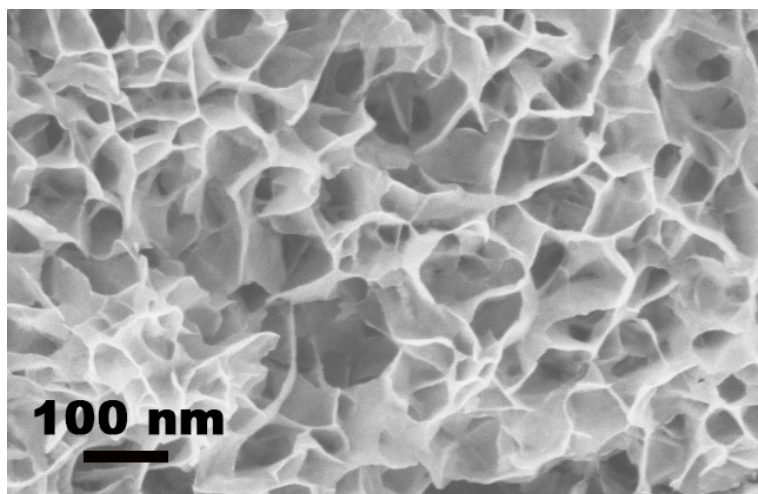


Fig. S1. SEM image for CoFe-LDH/NF.

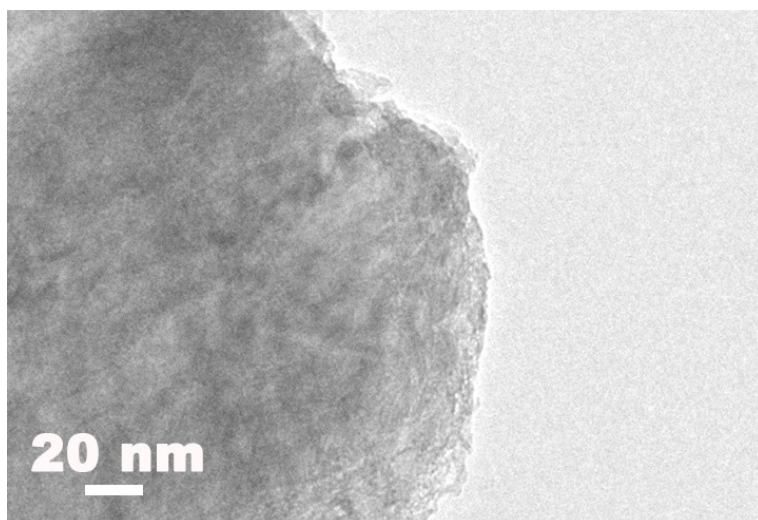


Fig. S2. TEM image for CoMoO₄.

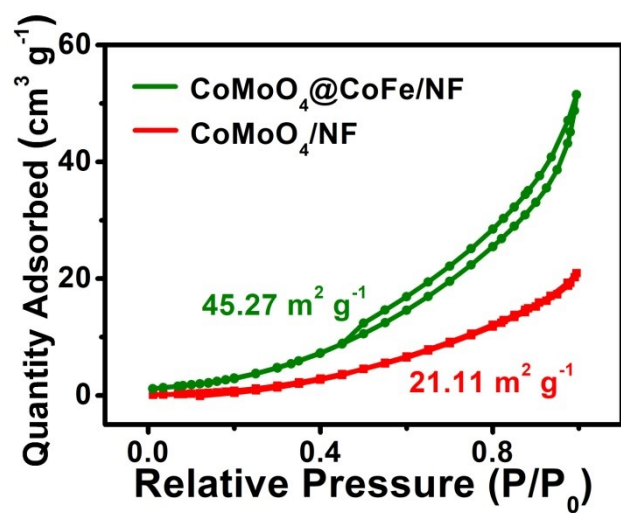


Fig. S3. N₂ sorption isotherms for CoMoO₄/NF and CoMoO₄@CoFe/NF.

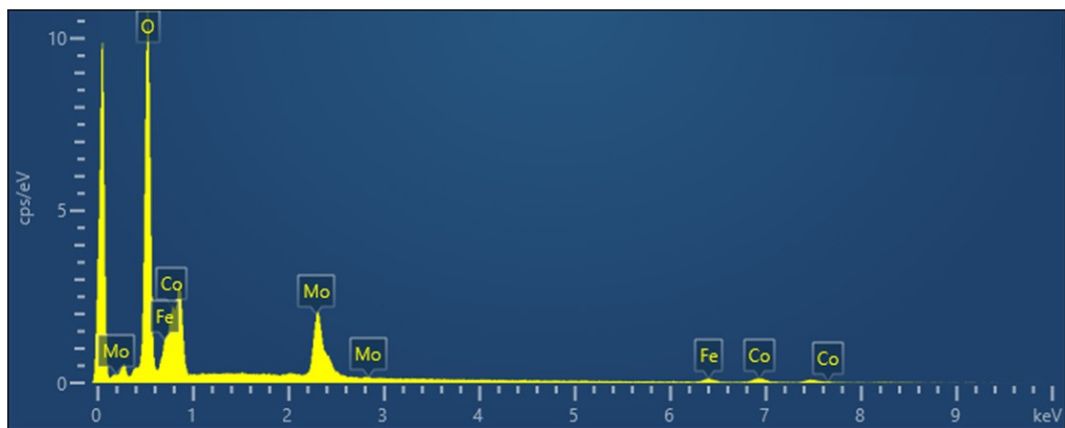


Fig. S4. EDX spectrum for $\text{CoMoO}_4@\text{CoFe/NF}$.

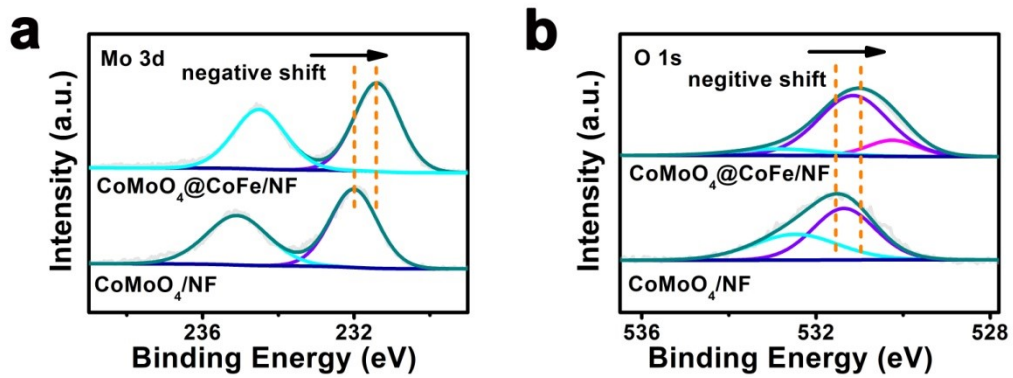


Fig. S5. (a) Mo 3d and (b) O 1s XPS spectra of CoMoO₄/NF and CoMoO₄@CoFe/NF.

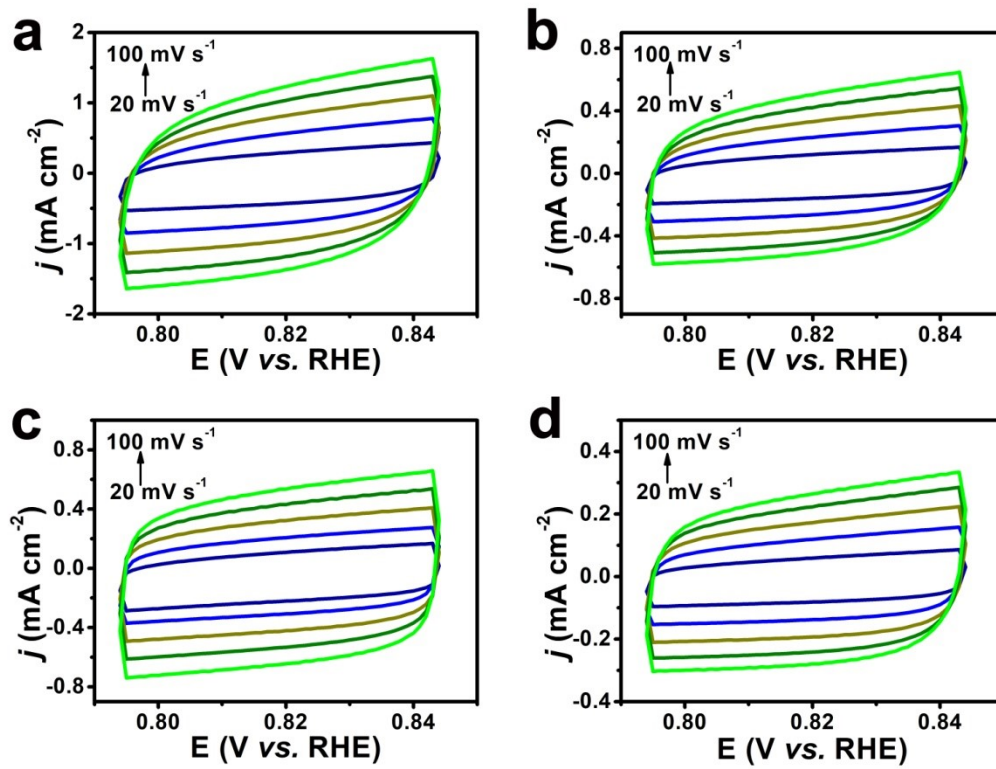


Fig. S6. CV curves for (a) $\text{CoMoO}_4@\text{CoFe}/\text{NF}$, (b) CoMoO_4/NF , (c) $\text{CoFe-LDH}/\text{NF}$ and (d) bare NF under different scan rates at different scan rates: 20, 40, 60, 80 and 100 mV s^{-1} from inside to outside.

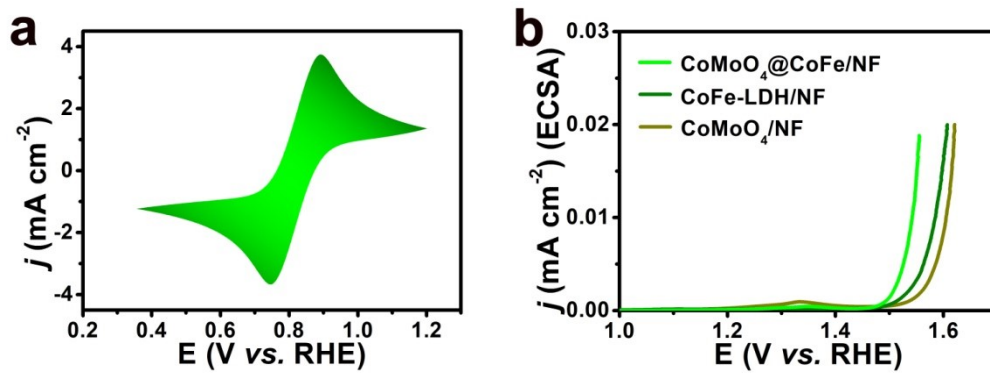


Fig. S7. (a) CV curve of bare NF recorded at a scanning rate of 10 mV s⁻¹ at 5 mM potassium ferricyanide; (b) LSV curves for CoMoO₄/NF, CoFe-LDH/NF and CoMoO₄@CoFe/NF with current density calculated by ECSA.

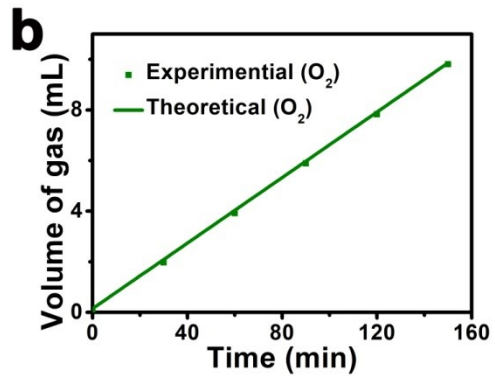
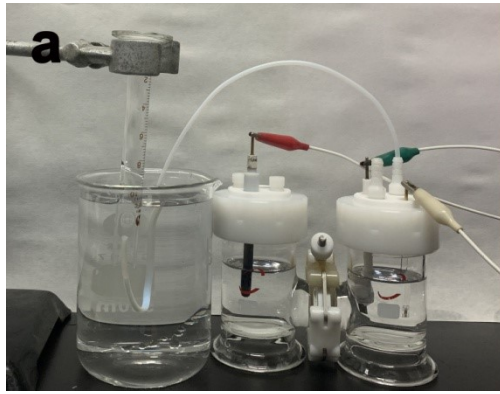


Fig. S8. (a) Optical photograph of a gas collection device. (b) The volume of O_2 theoretically calculated and experimentally measured under versus time on $CoMoO_4@CoFe/NF$.

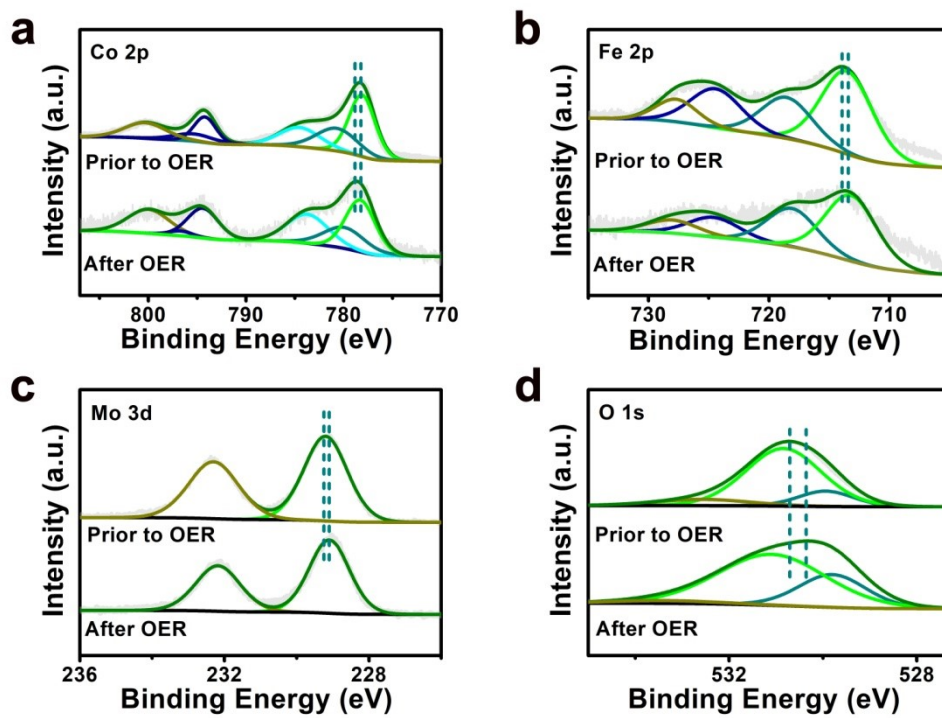


Fig. S9. The XPS spectra for CoMoO₄@CoFe/NF (a) Co 2p, (b) Fe 2p, (c) Mo 3d, (d) O 1s prior to and after OER test.

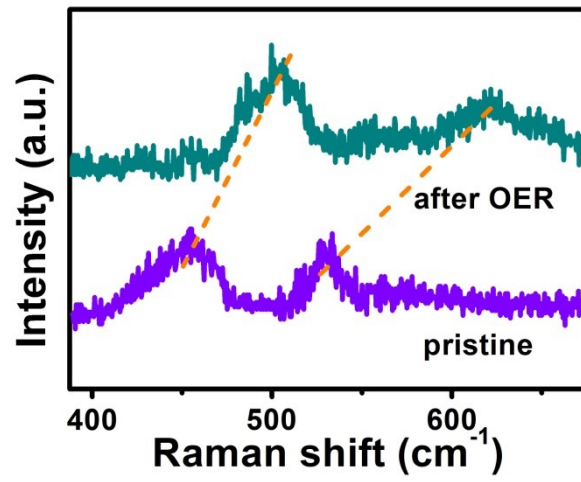


Fig. S10. Raman spectra for CoMoO₄@CoFe/NF prior to and after OER test.

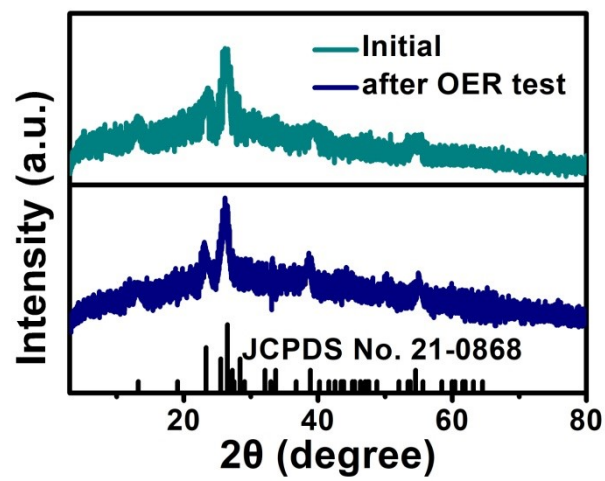


Fig. S11. XRD pattern for $\text{CoMoO}_4@\text{CoFe}$ prior to and after OER test.

Table S1. Atomic percentage of CoMoO₄@CoFe/NF.

Material	At%			
	Mo	Co	Fe	O
CoMoO₄@CoFe/NF	10.83	19.56	8.76	60.85

According to the EDX spectrum of CoMoO₄@CoFe/NF (Fig. S4), the corresponding atomic percentage of the CoMoO₄@CoFe/NF is shown in Table S1. The relative contents of CoMoO₄ and CoFe-LDH can be expressed as the percentage of Mo and Fe elements (CoMoO₄ : CoFe-LDH is 1.236).

Table S2. Comparison of OER performance between CoMoO₄@CoFe/NF and other OER electrocatalysts in alkaline media.

Catalyst	j (mA cm ⁻²)	η (mV)	Tafel polt (mV dec ⁻¹)	Electrolyte	Ref.
CoMoO₄@CoFe	10	245	46	1M KOH	This work
CoP NS	10	310	70.8	1M KOH	[1]
B- α -Co _{5.8} Fe LDH	10	264	34	1M KOH	[2]
NiCr-LDH	100	319	22.9	1M KOH	[3]
Mo-CoOOH,	10	305	56	1M KOH	[4]
Cu(OH) ₂ @NiFe-LDH	10	283	88	1M KOH	[5]
Fe/Zn-CoP	10	267	52.8	1M KOH	[6]
Co ₃ O ₄ /NiCo ₂ O ₄	10	320	89	1M KOH	[7]
Ni ₃ S ₂ @Co(OH) ₂	10	257	63.1	1M KOH	[8]
CoO _x /CoMoO ₄	10	253	75.8	1M KOH	[9]
(Ni,Co)Se ₂	10	256	74	1M KOH	[10]
CoMoO ₄ NAs	10	314	51	1M KOH	[11]
MoS ₂ /NiS ₂	10	249	57	1M KOH	[12]
NiFe ₂ O ₄	10	370	85	1M KOH	[13]
Co ₃ O ₄ @NiCoLDH	10	279	96.7	1M KOH	[14]
CoP@NC-3/1.	10	298	68.3	1M KOH	[15]

Reference

- 1 W. Zhu, W. Zhang, Y. Li, Z. Yue, M. Ren, Y. Zhang, N. M. Saleh and J. Wang, *J. Mater. Chem. A*, 2018, **6**, 24277–24284.
- 2 Y. Liu, Z. Jin, P. Li, X. Tian, X. Chen and D. Xiao, *ChemElectroChem*, 2018, **5**, 593–597.
- 3 W. Ye, X. Fang, X. Chen and D. Yan, *Nanoscale*, 2018, **10**, 19484–19491.
- 4 C. Guan, W. Xiao, H. Wu, X. Liu, W. Zang, H. Zhang, J. Ding, Y. P. Feng, S. J. Pennycook and J. Wang, *Nano Energy*, 2018, **48**, 73–80.
- 5 X. Ma, X. Li, A. D. Jagadale, X. Hao, A. Abudula and G. Guan, *Int. J. Hydrogen Energ.*, 2016, **41**, 14553–14561.
- 6 P. Wang, X. Liu, Y. Yan, J. Cao, J. Feng and J. Qi, *Catal. Tal. Sci. Technol.*, 2020, **10**, 1395–1400.
- 7 J. Béjar, L. Álvarez-Contreras, J. Ledesma-García, N. ArjonaL and G. Arriaga, *J. Electroanal. Chem.*, 2019, **847**, 113190.
- 8 S. Wang, L. Xu and W. Lu, *Appl. Surf. Sci.*, 2018, **457**, 156–163.
- 9 S. Xun, Y. Xu, J. He, D. Jiang, R. Yang, D. Li and M. Chen, *J. Alloy. Compd.*, 2019, **806**, 1097–1104.
- 10 W. Song, X. Teng, Y. Liu, J. Wang, Y. Niu, X. He, C. Zhang and Z. Chen, *Nanoscale*, 2019, **11**, 6401–6409.
- 11 H. Jiang, Z. Cui, C. Xu and W. Li, *Chem. Commun.*, 2019, **55**, 9432–9435.
- 12 Y. Yang, K. Zhang, H. Lin, X. Li, H. C. Chan, L. Yang and Q. Gao, *ACS Catal.*, 2017, **7**, 2357–2366.
- 13 A. Martínez-Lázaro, A. Rico-Zavala, F. I. Espinosa-Lagunes, J. Torres-González, L. Álvarez-Contreras, M. P. Gurrola, L. G. Arriaga, J. Ledesma-García and E. Ortiz-Ortega, *J. Power Sources*, 2019, **412**, 505–513.
- 14 R. Que, S. Liu, Y. Yang and Y. Pan, *Mater. Lett.*, 2021, **288**, 129364.
- 15 Q. Li, J. Hu, X. Wang, S. Yang, X. Huang and X. Cheng, *Appl. Surf. Sci.*, 2021, **569**, 151099.